LA-5131

C.3

Pressure Measurements on the Shock-Induced Decomposition of High-Density PETN

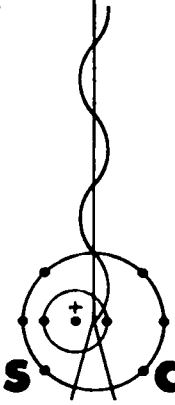

los alamos
scientific laboratory
of the University of California
LOS ALAMOS, NEW MEXICO 87544

UNITED STATES
ATOMIC ENERGY COMMISSION
CONTRACT W-7405-ENG. 36

Printed in the United States of America. Available from
National Technical Information Service
U. S. Department of Commerce
5285 Port Royal Road
Springfield, Virginia 22151
Price: Printed Copy $4.00; Microfiche $1.45

LA-5131
UC-34
ISSUED: November 1973

los alamos
scientific laboratory
of the University of California
LOS ALAMOS, NEW MEXICO 87544

Pressure Measurements on the Shock-Induced Decomposition of High-Density PETN

by

Jerry Wackerle
James O. Johnson

PRESSURE MEASUREMENTS ON THE SHOCK-INDUCED DECOMPOSITION OF HIGH-DENSITY PETN

by

Jerry Wackerle and James O. Johnson

ABSTRACT

Projectile impacts were used to generate planar shocks in disk-shaped 1.6- and 1.7-g/cm^3 pentaerythritol tetranitrate (PETN) pressings, and pressure histories were observed at both sample faces with quartz gauges. Input shock strengths ranged from 10 to 17 kbar, corresponding to 3.6 to 6.2 mm and 1.5 to 2.5 μsec for the shock to build up to detonation. There was no significant buildup of the shock front for the first 80% of its distance to detonation in 1.7-g/cm^3 samples, or for half of the run in 1.6-g/cm^3 pressings. In the higher density PETN, a pressure increase--ascribed to decomposition--occurs first near the impact face, producing a "following wave" which overtakes the shock front, corroborating observations made with the explosive wedge technique. Combined data from three shots on nominal 1.7-g/cm^3 PETN were treated with a direct analysis of the flow equations and simulated with a one-dimensional numerical hydrodynamic calculation. Both treatments gave wave structures and decomposition fields resembling those occurring in the shock initiation of homogeneous explosives, with complete reaction occurring near the impact face before the onset of detonation at the shock front.

I. INTRODUCTION

A realistic picture of the pressure waves produced in the buildup to detonation in solid explosives is of importance in treating practical shock initiation problems. The view that short run (< 10 mm) initiation of secondary heterogeneous explosives is controlled by decomposition very near the shock front has been supported by several studies using plane shock waves and streak-camera observations of wedge-shaped samples.[1-4] However, a growing body of evidence indicates that reaction occurring well behind the shock front has some role in the shock initiation of heterogeneous explosives. Some explosive wedge experiments have displayed wave-front velocities substantially exceeding detonation velocity at the onset of high-order detonation.[5,6] This "overshoot" phenomenon is characteristic of the shock initiation of homogeneous explosives, where reaction behind the front dominates the buildup.[7] Particle-velocity measurements show that substantial decomposition occurs in the interior of shocked TNT pressings,[8] and a similar behavior has been deduced for pressed pentaerythritol tetranitrate (PETN) from observations with instrumented gap tests.[9] Two experiments[10,11] have demonstrated that delayed decomposition is produced well behind the shock front in plastic-bonded HMX, and one investigator has recently concluded that this process effects its buildup to detonation.[12]

The 1.6- and 1.7-g/cm^3 pressed PETN used in this investigation has previously been the subject of a shock initiation study[13] with the explosive wedge technique. Overshoot was observed in most shots on the higher density pressings, and an additional feature of the streak-camera records was interpreted as manifesting a buildup dominated by a "second wave"--a reaction-induced disturbance formed behind the leading shock front--which overtakes the front and causes detonation. Neither phenomenon occurred with the 1.6-g/cm^3 PETN, and it was concluded that the buildup of this lower density explosive was more controlled by decomposition at the front.

This report presents results from a different experimental method for investigating the shock initiation of pressed PETN. The method uses projectile impacts to generate plane waves in disk-shaped PETN samples. Quartz gauges were used to monitor the pressures produced at the front, or impact, face and at the back surface of the pressings. This "front-back" technique[14] has been used extensively to study shock phenomena in inerts, in an initiation study similar to ours,[11,12] and in an earlier study of the shock properties of an explosive, but with stress levels below those producing prompt reaction.[15] The useful pressure limit of quartz gauges led us to restrict our study to the initial portion of the build-up process. In all cases, input shock strengths were chosen so that expected distance of run required to produce high-order detonation would exceed the sample thickness.

The experimental program was conducted as much to acquire and demonstrate the front-back technique on explosives as to obtain new information on the shock initiation of PETN. The program served the first purpose quite well, but had limitations that prevented a complete shock initiation study. Variations in sample densities, a narrow range of input shock strengths, and the small number of shots in the program kept the data from being definitive. Despite the limited scope of the experiments, pressure buildup from decomposition was observed, and the conditions and nature of its onset were defined to some extent. These observations are consistent with the conclusion that, in high-density PETN, reaction-induced pressure waves are generated well behind the shock front, and effect the relatively prompt onset of detonation when they overtake the shock front.

In Sec. II the experiments, their analyses, and some error sources are discussed, and methods are presented for calculating the shock parameters from gauge measurements. In Sec. III, principal results of the experiments are given and are compared with those obtained from the wedge technique. Estimates of the wave structures and reaction fields generated in a typical experiment are developed in Sec. IV, using two different methods of analysis. In Sec. V, these estimates are discussed and a specific feature of the observations is examined.

II. EXPERIMENTS AND ANALYSES

A. Experimental Arrangement

The impact experiments were performed on a modest gas gun having a 1.3-m-long barrel and a 51-mm-diam bore. The 9-liter breech volume was charged with helium at pressures up to 130 atm and the barrel and target chamber were evacuated to less than 0.01 torr. Projectiles were fired by the parting of break pins when sufficient breech pressure was attained. With the 136-g projectiles used, impact velocities up to 0.45 mm/μsec were obtained. The experimental arrangement used is displayed in Fig. 1.

Signals from a circular array of six electrical pin contactors were recorded on a raster oscilloscope to provide an impact velocity determination. Both the impacting projectile gauge and the target gauge were of the guard-ring type,[16] with 9.4-mm-diam electrodes. The projectile- and target-gauge elements were, respectively, 7.3 and 4.8 mm thick, yielding 1.23- and 0.84-μsec recording times. Each gauge was connected through 50-ohm impedance coaxial cable to two oscilloscope channels, and 50-ohm terminating resistors were used at one or both ends of the cables. The oscilloscopes were triggered by a signal from a pin contactor and, in most shots, another pin was used to record a common fiducial signal on all four scope channels, establishing the relative times of the impact-face and back-face measurements.

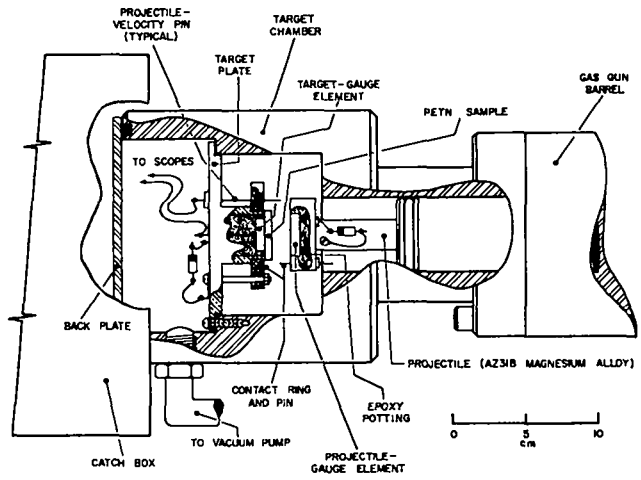

Fig. 1. Cutaway view of arrangement for front-back impact experiments.

B. Explosive Samples

The 33-mm-diam samples were pressed from PETN prepared with the same processing as the explosive used in our wedge-shot study[13] and in an earlier investigation of 1.0-g/cm^3 PETN.[2] Commercial-grade PETN was dissolved in acetone and precipitated with water, yielding very pure, elongated prismatic crystals with lengths ranging from 0.13 to 0.16 mm; air permeameter measurements gave a specific surface of about 3000 cm^2/g for the material. Sample disks were prepared in nominal 1.2-, 1.9-, and 4-mm thicknesses with nominal 1.6- and 1.7-g/cm^3 densities. The control of the pressing density was not particularly good, and a variation of 0.03 g/cm^3 occurred among higher density samples, with the thicker pressings having the lower density. Samples with faces machined flat and parallel were used in the majority of shots reported here; the thickness of the remaining pressings varied as much as 0.05 mm across a diameter.

C. Projectile Velocity and Gauge Pressure Analyses

Projectile velocities were determined by least-squares fitting of a linear distance-time relation to the velocity-pin data. A measure of their accuracies was provided by the standard deviations obtained in the least-squares calculation, and was usually less than 1% of the calculated velocities. The deviations of the individual pin signal times from the corresponding calculated times gave an estimate of the overall tilt of the projectile relative to the reference surface of the target assembly.

Figure 2 shows a typical set of oscilloscope records for the experiment. These records were read on a digitized comparator and a code for a CDC 6600 computer was used for reducing the quartz-gauge data. Voltages and times were determined by a calibration technique that involved recording a voltage-time grid for each oscilloscope beam and least-squares fitting of the voltage and times to a polynomial in both film coordinates. Pressures at the gauge-sample interfaces were computed using relations established at Sandia Laboratories[16,17] for both the Hugoniot of x-cut quartz* and the coefficient

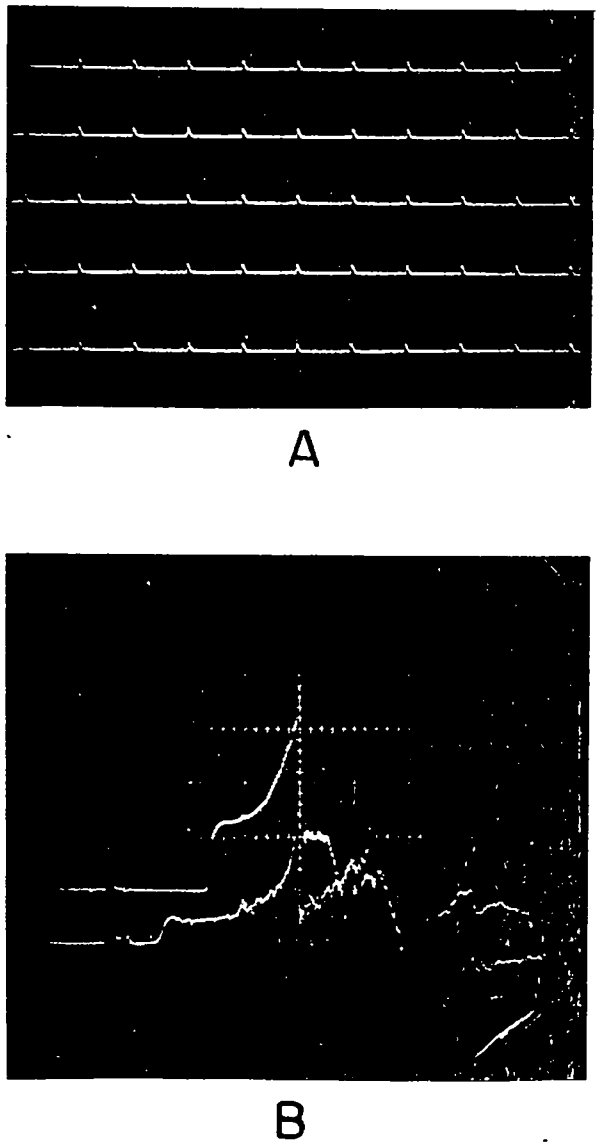

Fig. 2. Typical calibration grid (above) and oscilloscope traces of quartz-gauge records in front-back experiments. Records shown were obtained on a Tektronix Model 556 dual-beam oscilloscope. The calibration grid is for the upper trace of the pair below, with 0.5-μsec time marks and approximately 14 V between traces. The lower of the pair of gauge records is from the impact face, and was taken with the same sweep speed and voltage sensitivity as the target gauge measurement. Useful data from each gauge end at about the center of the record. The common time fiducial signal is evident at the left side of each trace. The data shown were for Shot 7-7, which is displayed in reduced form in Fig. 4.

*The Hugoniot for the elastic compression of x-cut quartz was represented by relations for the shock velocity, U_q, as function of particle velocity, u_q, as U_q = constant = 5.7211 mm/μsec for stresses below 21.5 kbar, and at higher pressures $U_q = 5.57 + 1.08\ u_q$ mm/μsec which, except for a lower changeover stress, is the same as reported in Ref. 16.

relating stress to gauge current.* A first-order correction for finite strain of the gauge elements was included in the analysis. For our data, this correction typically reduced pressures about 3% near the end of the gauge recording time. Typical results from the data reduction are displayed in Figs. 3 and 4.

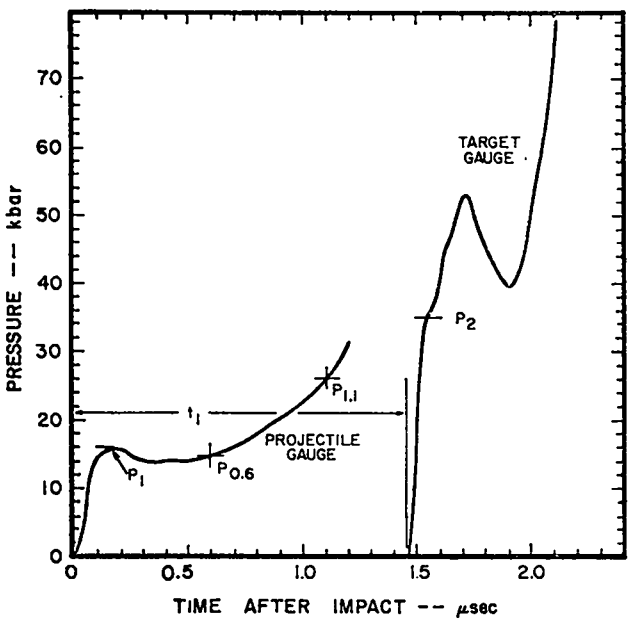

Fig. 3. Typical pressure profiles from front-back experiment on a thick PETN sample. Various parameters determined from the reduced gauge records are indicated. The profiles are for Shot 7-9, which had a 3.95-mm, 1.69-g/cm^3 sample.

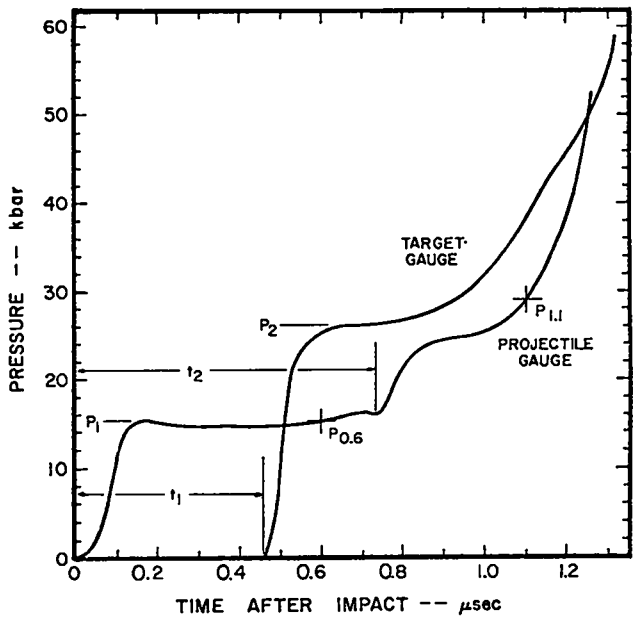

Fig. 4. Typical pressure profiles from a front-back experiment on a thin sample. The reduction displayed is for the oscilloscope traces shown in Fig. 2. Some smoothing of the data is evident, and was accomplished primarily in the film reading. The Shot 7-7 shown was with a 1.22-mm, 1.70-g/cm^3 PETN pressing.

D. Measurement Inaccuracies and Anomalies

Projectile tilts determined from velocity-pin data were generally about 10^{-3} rad. The risetimes on the quartz-gauge traces generally were about 0.1 μsec, which (with the gauge dimensions and projectile velocities used) corresponded to tilts of around 4×10^{-3} rad. The pin data analysis gave the tilt of the target-plate face relative to the projectile rim, and it was possible for the gauge elements to be tilted relative to these reference surfaces (see Fig. 1). The aplanarity of some of the samples could also contribute to risetimes. Preshot measurements seldom revealed misalignments of the assemblies that could give the tilts indicated by the gauge records, but such misalignments--perhaps aggravated during the projectile travel down the barrel--are still considered a more likely cause of the slow risetimes than is a hypothetical anomalous compression property of pressed PETN.

Poor geometrical design, allowing trailing or side rarefactions to encroach into critical sample areas during the pressure measurement period, and a variety of effects that can occur in the use of

*The coefficient k relates the stress at the gauge interface, σ, to the current, represented by V/R, by:

$$k\sigma = \frac{V}{R} \cdot \frac{\ell}{AU_q}$$

where A and ℓ are, respectively, the signal electrode area and the thickness of the gauge. The dependence of k on stress:

$k = (2.01 \times 10^{-8}) + (1.1 + 10^{-10})\ \sigma$ (C-cm^{-2}-kbar^{-1})

is reported in Ref. 17.

quartz gauges are frequent sources of spurious results in front-back experiments. Care in choosing the dimensions of our gauges and samples eliminated misinterpretations from the first cause. However, some error sources remain in the quartz-gauge determinations: effects of electric field distortion, effects of stress levels exceeding those for an elastic dynamic response in the quartz, and the effect of electric conduction in the crystal.

Even at very low stress levels, precise pressure determinations with quartz gauges require that the electric field lines encompassed by the measuring electrode be exactly parallel to the axis of the disk-shaped element. When the gauge is surrounded by a grounded, conducting cylinder, as in our configurations, some degree of deviation from the parallel condition will occur, and the response of the gauge will have some degree of error. The resulting signal distortion yields apparent pressures that are below the actual values initially, and that are higher by a similar amount near the end of the gauge recording time. As has been described by Reed,[18] gauges with electrode diameters a sizable fraction of that of the grounded shields can yield pressures that are incorrect by as much as a factor of two. For our gauge configurations, this problem is far less serious. Electrostatic analysis[19] and quartz-quartz impact experiments at appropriate shock strengths (17 kbar for the projectile gauge and 25 kbar for the target) have demonstrated that an error of less than 3% is introduced by electric field distortion with our gauge configurations. No correction is made for this effect in our analyses.

A well-defined piezoelectric response of quartz gauges requires that the element be compressed "elastically," with the proper anisotropic stress configuration. This condition can be sustained only at limited shock strengths. Shock compression studies have shown[20] that shock waves up to 80 kbar will induce this elastic stress configuration in x-cut quartz initially, but at these pressures a subsequent stress relaxation to a more isotropic, lower pressure state occurs on a tenth-microsecond time scale. This relaxation in the gauge element does not seriously affect the initial rise in its signal if the stress loading is sufficiently abrupt; however, the later portion of the waveforms may be distorted to indicate lower-than-actual pressures. Graham and Ingram[21] detected this effect at stresses above 25 kbar and substantial distortions were produced at pressures above 40 kbar. In our experiments, stress relaxation probably does not introduce any inaccuracy in the initial shock pressures determined with the gauges, but may well have produced apparent pressures a few percent below the actual values in later portions of most of the target-gauge observations, and of such projectile-gauge measurements as are shown in Fig. 4.

Possible dielectric breakdown and conduction within quartz gauges provide the most serious problems, as these phenomena occur quite erratically and may lead to gross misinterpretations when they do. One instance of an effect of finite conductivity in the gauge element is the so-called "short pulse anomaly," in which a signal from a pressure pulse of duration less than the gauge transit time is followed by a completely spurious signal indicating a pressure excursion. The final pressure excursion in the target-gauge record of Fig. 3 could be a result of such behavior. Graham and Ingram[22] investigated this anomaly, and established that its onset correlates with a reverse electric field exceeding 2.8×10^5 V/cm in the portion of the gauge behind the pulse. Analysis reveals that this criterion was not met in our shots. However, it should be noted that Graham and Ingram's conditions for the anomaly are established only for very ideal input pressure pulses and for substantially lower stress levels than occur in our experiments.

In impact experiments not otherwise discussed here, we obtained target-gauge signals with a "hump" similar in shape and amplitude to that shown in Fig. 3, and it was known that the shock in the PETN had built up to detonation before reaching the gauge. Because of such observations, and recognizing the uncertainty in quartz-gauge response to complex stress inputs above 40 kbar, we are not certain whether such observations accurately depict the pressure history.

E. Measurements of Shock Parameters

Some shock parameters directly measured in the experiments are indicated in Figs. 3 and 4 and listed later in Table III. The peak of the first rise of the projectile-gauge profile, P_1, is the initial shock pressure in the explosive sample. Typically, the impact-face profiles display

slightly decreasing pressure for about 0.3 to 0.5 μsec, and then show varying degrees of pressure increase. Some measure of this behavior was obtained by evaluating the pressures, $P_{0.6}$ and $P_{1.1}$, at 0.6 and 1.1 μsec after impact.* The pressure at the first "knee" in the target-gauge profiles, P_2, is the reflected-shock pressure associated with the shock front incident on the gauge. The transit time, t_1, through the sample was obtained by comparing the start of the two gauge records (using a common fiducial signal), and, using the known sample thickness, d, an average shock velocity, $\bar{U}_1$, through the pressing was calculated. With thinner samples, the shock reflected from the target gauge reached the projectile gauge while it was still recording; this arrival was manifested by a pressure step, shown at a time t_2 in Fig. 4. With the 1.2-mm explosive thickness, the wave interaction at the projectile gauge produced a second reflected shock which reached the target gauge about 0.5 μsec after it began recording. The pressure jump associated with this reverberation was only about 3 kbar, and it reached the back face during a period when the signal was rapidly increasing for other reasons. This second reverberation was neither discernible on the gauge records nor considered in the analyses and interpretations.

The shock pressures, the projectile velocity, V, the sample initial density, ρ_0, the known Hugoniot for x-cut quartz, and the shock conservation relations are sufficient to complete the determination of the initial- and reflected-shock parameters. As indicated in Fig. 5, the initial particle velocity, u_1, in the sample is established by the initial pressure on the Hugoniot for the quartz projectile face (and the condition that pressure and particle velocity are continuous across a contact surface). The initial shock velocity, U_1, and shocked density, ρ_1, follow from the conservation relations:

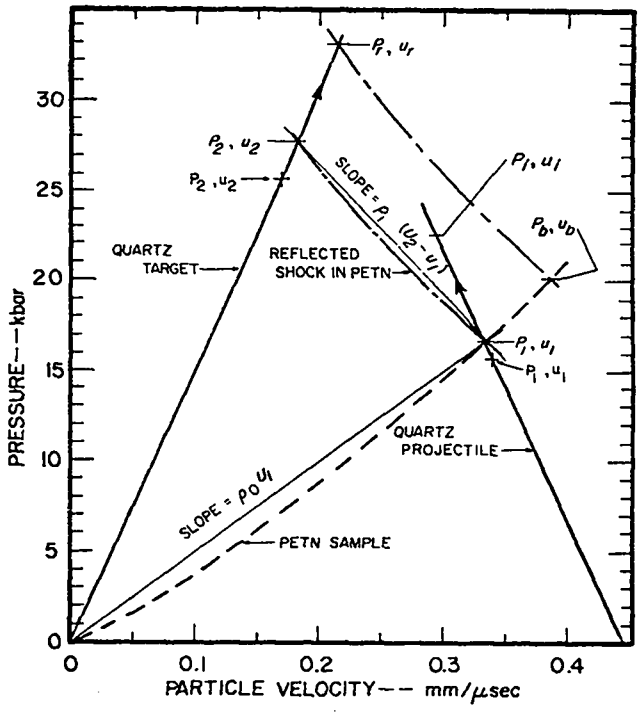

Fig. 5. Typical impedance-match solution for calculated and observed shock states in front-back experiments. The PETN Hugoniots are those developed from wedge-shot data and the Mie-Grüneisen equation of state, as described in the text, and the intersections and slopes indicated with italicized notation are the calculated expected values of the shock parameters. The quantities P_1 and P_2 are the initial pressure determinations with, respectively, the projectile and target gauges; constructions similar to those shown would yield the "observed" first and reflected shock velocities. The solutions are for Shot 7-7, also the subject of Figs. 2 and 4. The significance of the parameters subscripted *r*, *b*, and *i* is discussed in Sec. IV.

$$P_1 = \rho_0 U_1 u_1$$

and

$$\frac{\rho_1}{\rho_0} = \frac{U_1}{U_1 - u_1} .$$

Similar considerations give the parameters behind the reflected wave.

Values of P_1 and P_2 were obtained by examining the graphical output of the analysis code and scaling off the desired parameter--a procedure that involves some judgment. Additional error sources, such as field fringing, the measurements of gauge dimensions and terminating resistors, and

*For the purpose of these evaluations and the transit time measurements, time of impact was defined as the first detectable rise of the projectile-gauge signal. With the finite risetimes caused by tilt, the midpoints of initial rising portions of the traces, representing the impact time at the centers of the gauges, could have been a better choice for this determination in principle, but in practice was usually more difficult to define.

comparisons of dual observations of the same signals contribute to a total estimate of about ±5% error in the pressure measurements. The projectile-velocity and sample-density determinations were relatively accurate, so the values obtained for u_1 and U_1 also have about ±5% error. The transit-time measurements have estimated errors of ±0.05 μsec, which results in errors approaching 10% for determinations of $\bar{U}_1$ for thinner samples.

F. Calculation of Shock and Initiation Parameters Predicted by Wedge Experiments

To interpret our observations with front-back experiments, it is desirable to know at what stage in the buildup process the pressure measurements were obtained. The wedge-experiment data are available for this purpose but, as noted in Ref. 13, measurements of the input shock strengths in that program were somewhat inaccurate, producing both ill-determined Hugoniots for the explosives, and uncertainties in the correlations of the times and distances of buildup to detonation to the initial shock pressure. These uncertainties are heightened by the fact that front-back experiments were conducted at lower input shock strengths than most of the wedge shots, so that the estimates presented below generally represent some extrapolation of the earlier data.

For the sake of consistency, the input shock strengths for the computations of expected times and distances to detonation were developed from the wedge-shot data. More recent Hugoniot data for 1.75-g/cm^3 PETN led us to reformulate the Hugoniot for 1.72-g/cm^3 PETN. A linear relation between the shock and particle velocity was used, with the shock velocity constrained to equal the bulk sound speed at zero particle velocity.* Least-squares analysis of this U-u relation gave:

$$U = 2.326 + 2.342\,u \qquad \text{(mm/μsec)};$$

which yields

$$P = 40.00\,u + 40.28\,u^2 \qquad \text{(kbar)}.$$

*The bulk sound speed used, 2.326 mm/μsec, was determined from longitudinal and shear sound speed measurements of, respectively, 2.933 and 1.547 mm/μsec, recently obtained for 1.72 g/cm^3 PETN by C. E. Morris of Group M-6. The unconstrained Hugoniot representation reported in Ref. 13 was $U = 1.83 + 3.45\,u$.

For PETN with initial densities other than 1.72 g/cm^3, Hugoniots were calculated using the above representation as a reference curve and the Mie-Grüneisen equation of state, with the product of the Grüneisen ratio, Γ, and density assumed constant:[23]

$$\frac{1}{\rho\Gamma} = \Omega = \left(\frac{\partial E}{\partial P}\right)_\rho = \frac{C_p}{\rho_o \beta\, c^2} \qquad (\text{cm}^3/\text{g}),$$

where E is the specific internal energy. A value of Ω of 0.50 cm^3/g was determined from the indicated combination of the bulk sound speed, c, specific heat, C_p,[24] and thermal expansion, β.[25]

PETN Hugoniots were constructed in the pressure-particle velocity plane and the expected values of P_1, u_1, and U_1 determined by impedance-match solution with the quartz Hugoniot centered at the projectile velocity (see Fig. 5). The equation-of-state assumptions described were also used to construct reflected-shock Hugoniots for PETN. These Hugoniots were then used to obtain expected initial pressures at the target gauge, P_2, assuming that no buildup of the incident wave had occurred. The additional assumption[26] of constant specific heat at constant volume, equal to 1.003 J/g-°K,[24] was imposed to calculate the increase in sample "bulk temperature" (that is, considering the explosive as a homogeneous fluid). For these calculations the initial temperature was taken to be 300°K in all instances.

As in Ref. 13, the linear log-log form of Ramsey and Popolato[27] was employed for the buildup relations between P_1, the distance, D, and the time, T, to detonation. New computations of the buildup relations gave the results listed in Table I. With the rationale that better fitting of the data would be obtained by minimizing the variance of the less accurately measured parameter, the least-squares analyses of the relations involving pressures were actually performed on the inverted forms of the equations shown in Table I, with P_1 used as the dependent variable. This change from former practice, and the discovery of some errors in the previous determination of D (see Fig. 6) account for the difference in the coefficients listed here and in Ref. 13.

TABLE I

RELATION BETWEEN BUILDUP PARAMETERS FOR 1.6- AND 1.72-g/cm^3 PETN

The coefficients listed were determined by nonlinear least-squares fitting of the data of Ref. 13, and have dimensions appropriate for D in mm, T in μsec, and P_1 in kbar.

Initial Density (g/cm^3)	Formulation	A	B
1.6	$D = AT^B$	2.585	0.890
	$D = AP_1^{-B}$	567.1	1.985
	$T = AP_1^{-B}$	390.3	2.196
1.72	$D = AT^B$	3.209	0.850
	$D = AP_1^{-B}$	593.2	1.678
	$T + AP_1^{-B}$	487.2	1.989

To provide estimates of the times and distances to detonation for explosive samples of densities different from 1.6 and 1.72 g/cm^3, an arbitrary linear relation to initial density was assumed for both coefficients, that is:

$$A = A_0 + A_1 \rho_0$$

$$B = B_0 + B_1 \rho_0 \quad .$$

The information in Table I and simple algebraic solutions provided the values of the coefficients listed in Table II. A feeling for the initial-density "correction" can be found in Fig. 6, where the cross-hatched curve depicts the variation of the calculated times and distances to detonation with initial density for a constant, 15 kbar, input shock strength. As earlier work has demonstrated,[1] the effect of sample density is quite substantial. For instance, in the higher density region of the case illustrated, a 2% reduction in ρ_0 shortens the distance to detonation as much as a 17% increase in input shock pressure. Such striking examples demonstrate the need for some correction for initial density or, preferably, more uniformity of samples.

All of the estimates of predicted shock and buildup parameters were based on new analytic representations of the wedge-shot data. Computations of the expected parameters were also made using the

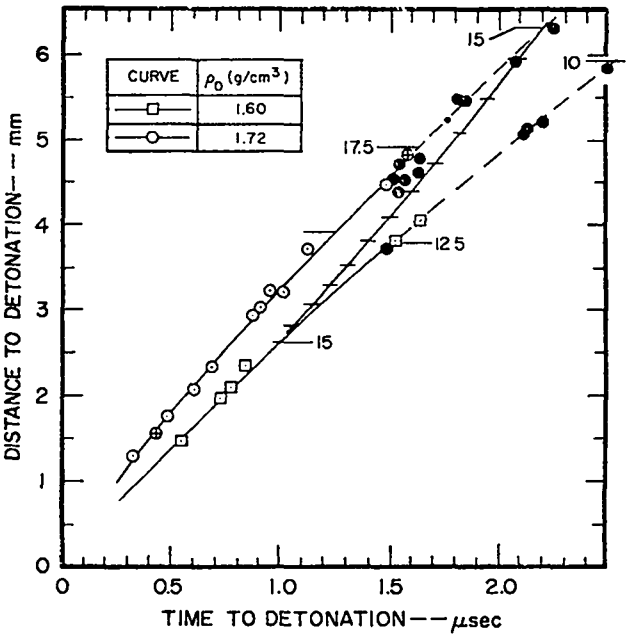

Fig. 6. Buildup data from explosive wedge experiments. Wedge-shot determinations of times and distances to detonation for 1.6 and 1.72 g/cm^3 are fitted with curves with the analytic forms and coefficients listed in Table I. The crossed-circle symbols denote points with ordinates corrected from those listed in Ref. 13, and the numerical labels along the curves show the input shock pressures (in kilobars) yielding the indicated times and distances to detonation. The cross-hatched curve represents the values of D and T expected with a 15-kbar input shock and intermediate densities; the cross hatches are located at 0.01-g/cm^3 density increments. The solid symbols represent the expected distances and times to detonation calculated for the front-back experiments.

TABLE II

CONSTANTS FOR INTERPOLATION OF BUILDUP COEFFICIENTS WITH DENSITY

Values are for parameter dimensions as described in Table I.

Formulation	Coefficient	A_0 or B_0	A_1 or B_1
$D = AP_1^{-B}$	A	219.1	217.5
	B	6.083	-2.561
$T = AP_1^{-B}$	A	-900.9	807.0
	B	4.969	-1.733

U-u and D-P relations given in Ref. 13. With the previous representations, the estimated first-shock strengths were generally 2 to 3% less than, the reflected-shock pressures 4 to 5% greater than, and distances and times to detonation 10 to 15% larger than those listed in Table III. Such differences reflect the magnitude of uncertainty arising from the wedge experiments, but, fortunately, in no way alter the principal interpretations and conclusions of the following sections.

III. PRINCIPAL OBSERVATIONS

A. Comparisons of Observed and Predicted Shock Parameters

The shock parameters determined in the front-back experiments and those calculated from wedge-shot data are listed in Table III. The principal comparisons available in the tabulation are of the initial shock pressures, P_1 and $\mathcal{P}_1$, the reflected-shock pressure, P_2 and $\mathcal{P}_2$, the three different determinations of first-shock velocity, U_1, $\overline{U}_1$, and $\mathcal{U}_1$, and, for shots with thinner samples, the reverberation times, t_2 and $\mathcal{t}_2$.

Only about half of the experimental and calculated first-shock pressures for nominal 1.7-g/cm^3 PETN agree within the 5% measurement error, and a definite bias of the quartz-gauge measurements yielding lower pressures is discernible. With one exception, the agreement for 1.6-g/cm^3 samples is well within experimental error, and the slight bias is to higher, rather than lower, measurements. The substantially larger disagreements between P_1 and $\mathcal{P}_1$ (and the unreasonable values of U_1) in Shots 7-10 and 6-3 strongly suggest that some gross experimental error was made in the quartz-gauge measurements, such as inaccurate determinations of terminating resistors, calibration voltages, etc. Otherwise, the differences are more likely due to poor choice of equation-of-state representations for the computed shock pressures than to some consistent error in the gauge measurements.

As will be discussed, some experiments (7-3, 7-9, 6-1, 6-2, 6-4) with sample thicknesses a sizable fraction of the distance to detonation (that is, $R = d/D$ approaching unity) should not be included in comparing the observed and calculated reflected-shock pressures. The majority of the remaining comparisons of P_2 and $\mathcal{P}_2$ agree within estimated experimental error, with the calculated values generally being slightly larger. This is again believed due to the choice of equation-of-state representation. Note, however, that use of the Hugoniot relation of Ref. 13 for the reference locus in the calculation, while improving the agreement of the first-shock pressures, would worsen that for the reflected-shock determinations.

Except for Shots 7-10 and 6-3, the average first-shock velocities, $\overline{U}_1$, generally agree with the values of U_1 derived for the impact-face pressure measurement within experimental error. The size of the error and scatter permits no significant conclusions from this comparison. In particular, there is no consistent tendency to find $\overline{U}_1 > U_1$, which would indicate acceleration of the wave during run; if anything, the opposite is true. While agreeing within experimental error, the calculated values, $\mathcal{U}_1$, tend to be somewhat larger than the corresponding observations, as would be expected from similar comparisons of the first-shock pressures.

The reverberation times for thinner samples (Shots 7-4, -5, -6, -7, -8, -9, and 6-3 and -5) agreed within experimental error, and gave no information other than to confirm that the reflected waves were properly identified.

Overall, the agreement between parameters determined by the front-back technique and wedge-shot experiments is quite adequate, so that the quartz-gauge observations can be sensibly discussed in terms of the expected times and distances to detonation.

B. Impact-Face Pressures in 1.7-g/cm^3 PETN

Figures 7 and 8 display a collection of projectile- and target-gauge pressure profiles for nominal 1.7-g/cm^3 PETN that illustrate most of the qualitative conclusions of this report. Figure 7 is a comparison of profiles obtained with thick samples over a rather narrow range of input shock strengths. Figure 8 shows profiles obtained with different thicknesses of PETN shocked to approximately the same initial pressure.

In both figures and in nearly all the observations of this study, the projectile-gauge records displayed a relaxation in pressure following the initial rise to P_1. The pressure decrease was typically about a kilobar and occurred in 0.2 to 0.5 μsec. Generally, by 0.6 μsec after impact the

TABLE III

RESUMÉ OF OBSERVATIONS AND CALCULATED SHOCK AND INITIATION PARAMETERS FOR 17 FRONT-BACK EXPERIMENTS ON 1.6- AND 1.7-g/cm^3 PETN

The symbols denoting the various parameters are identified in the text. Numbers obtained from calculations based on wedge-shot experiments (Ref. 13) are italicized.

	Initial Conditions			First Shock										Reflected Wave			
Shot No.	ρ_o (g/cm^3)	d (mm)	V (mm/μsec)	u_1	U_1	$\bar{U}_1$	U_1 (mm/μsec)	P_1	P_1	$P_{0.6}$	$P_{1.1}$ (kbar)	ρ_1 (g/cm^3)	T (μsec)	D (mm)	R	P_2	P_2 (kbar)	t_2	t_2 (μsec)
7-1	1.71	4.45	0.384	N.O.[a]	N.O.	N.O.	*2.92*	*14.4*	N.O.	N.O.	N.O.	N.O.	*2.27*	*6.28*	*0.71*	*23.7*	24.3	N.O.	*2.62*
7-2	1.71	4.45	0.398	0.302	2.83	2.82	*2.94*	*15.0*	14.6	13.6	15.1	1.91	*2.09*	*5.84*	*0.76*	*24.6*	23.8	>1.23	*2.59*
7-3	1.72	4.45	0.429	0.326	2.78	2.95	*3.07*	*16.8*	15.6	14.8	21.9	1.96	*1.78*	*5.21*	*0.85*	*27.1*	33.8	>1.23	*2.49*
7-4	1.73	1.27	0.427	0.317	3.05	N.O.	*3.15*	*17.1*	16.7	15.1	25.5[b]	1.93	*1.83*	*5.45*	*0.23*	*27.1*	28.0	0.73	*0.70*
7-5	1.72	2.03	0.421	0.310	3.18	N.O.	*3.05*	*16.4*	16.8	15.0	19.8	1.91	*1.86*	*5.41*	*0.37*	*26.5*	25.9	1.18	*1.14*
7-6	1.69	4.06	0.433	0.332	2.73	2.68	*2.86*	*15.8*	15.3	15.0	21.2	1.97	*1.65*	*4.59*	*0.88*	*26.8*	N.O.	N.O.	*2.37*
7-7	1.70	1.22	0.444	0.342	2.65	2.71	*2.95*	*16.7*	15.4	15.0	29.0[b]	1.95	*1.58*	*4.51*	*0.27*	*27.8*	26.0	0.73	*0.70*
7-8	1.71	1.91	0.440	0.337	2.70	2.98	*3.01*	*16.9*	15.6	15.5	24.4	1.96	*1.65*	*4.77*	*0.40*	*27.7*	25.6	1.12	*1.07*
7-9	1.69	3.95	0.444	0.340	2.75	2.71	*2.87*	*16.3*	15.8	14.2	25.3	1.93	*1.55*	*4.35*	*0.91*	*27.7*	35.0	>1.23	*2.28*
7-10[c]	1.71	1.23	0.453	0.355	2.45	2.92	*3.03*	*17.5*	14.9	15.0	18.8[b]	1.99	*1.53*	*4.50*	*0.27*	*26.7*[c]	24.3[c]	0.68[c]	*0.72*[c]
7-11[c]	1.72	1.90	0.451	0.343	2.71	2.97	*3.11*	*18.0*	16.3	16.2	20.8[b]	1.96	*1.56*	*4.66*	*0.41*	*27.1*[c]	24.6[c]	1.05[c]	*1.06*[c]
7-12[d]	1.71	1.23	0.453	0.344	2.80	2.99[d]	*3.03*	*17.5*	16.5	15.8	16.2[b]	1.95	*1.53*	*4.50*	*0.27*	*0.0*[d]	N.O.	0.70[d]	*0.72*[d]
6-1	1.58	4.45	0.355	0.290	2.16	2.04	*2.04*	*9.4*	9.9	9.6	9.8	1.82	*2.51*	*5.83*	*0.76*	*19.6*	29.0	>1.23	*3.31*
6-2	1.60	4.39	0.375	0.305	2.17	N.O.	*2.19*	*10.7*	10.6	10.4	10.8	1.86	*2.15*	*5.16*	*0.85*	*21.3*	29.2	>1.23	*3.09*
6-3	1.58	1.23	0.370	0.293	2.52	2.08	*2.08*	*10.0*	11.7	9.0	17.5[b]	1.79	*2.21*	*5.19*	*0.24*	*21.2*	19.8	0.92	*0.90*
6-4	1.59	4.23	0.375	0.304	2.23	2.00	*2.14*	*10.4*	10.8	9.6	10.4	1.84	*2.13*	*5.07*	*0.83*	*21.2*	32.5	>1.23	*3.02*
6-5	1.59	1.23	0.421	0.339	2.30	2.13	*2.25*	*12.2*	12.4	11.4	23.4[b]	1.87	*1.50*	*3.68*	*0.33*	*24.4*	23.3	0.87	*0.83*

[a] N.O. indicates measurement not obtained.

[b] Pressure value affected by reflected wave.

[c] Shot assembly included 0.82-mm-thick Lucite buffer between the PETN sample and target gauge. The reflected waves observed and calculated were rarefactions from the PETN-Lucite interface, and the value of P_2 is for the shock reflected into the Lucite by the target-gauge element.

[d] No target gauge was used in this shot, and the transit time was measured with a ferroelectric pin. The reflected wave was the rarefaction from the sample's free surface.

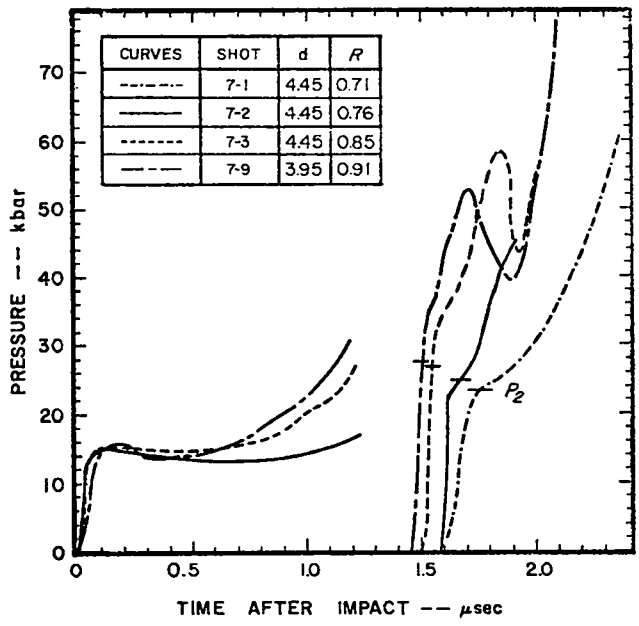

Fig. 7. Comparison of pressure profiles from thick samples with varied input shock strength. The observed input shock strengths on Shots 7-2, -3, and -9 were, respectively, 14.6, 15.6, and 15.8 kbar. (The projectile-gauge record on Shot 7-1 was lost, but, based on projectile velocity, an initial pressure about 0.5 kbar less than Shot 7-2 must have been generated.) The cross-hatch marks on the target-gauge profiles indicate the expected reflected-shock pressure, P_2, calculated with the assumption of no buildup.

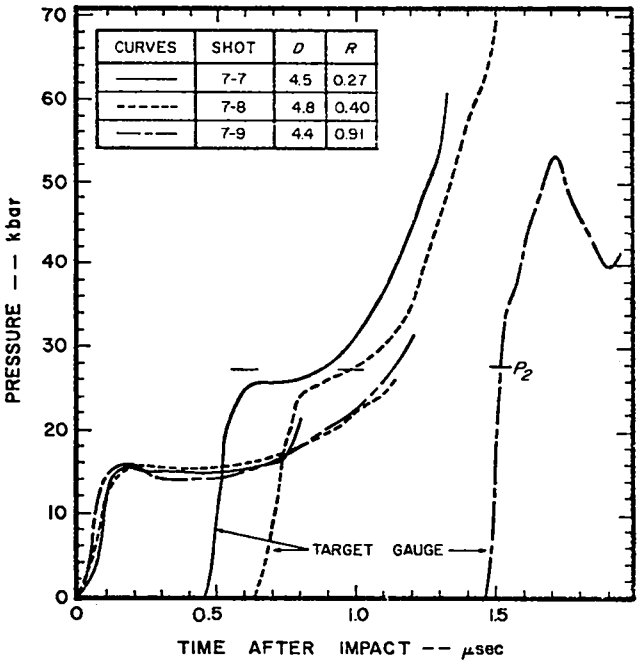

Fig. 8. Comparison of pressure profiles from various thickness samples and the same nominal input shock strength. Sample thicknesses in Shots 7-7, -8, and -9 were, respectively, 1.22, 1.91, and 3.95 mm.

projectile gauge is still registering a pressure less than the initial value (see Table III).

Typically, the impact face pressures for 1.7-g/cm^3 PETN begin to display some degree of increase between 0.4 and 0.6 μsec after impact. As shown in Fig. 7, the extent of the pressure excursion (during the gauge recording time) is quite sensitive to the input shock strength, varying almost an order of magnitude with a 10% change in impact velocity. Figure 8 shows that similar projectile-gauge pressure excursions are produced in experiments with about the same shock inputs.* Except where identified as resulting from reflected shocks, the pressure increases at the impact face are concluded to be caused by reaction induced in the explosive.

*For samples with different initial densities, the "same" shock input is probably best defined as "that shock strength giving the same distance to detonation."

C. Back-Face Pressure Profiles for 1.7-g/cm^3 PETN

Figures 7 and 8 show two distinct forms of target-gauge pressures characteristic of those obtained. The type observed has a definite correlation to the ratio of the sample thickness to the expected distance to detonation (the parameter R).

In all experiments with $R < 0.8$, profiles such as shown for Shot 7-1 were obtained. Examination of the figures and Table III reveals that the observed initial reflected-shock pressures, P_2, in these cases were about the same as the values of P_2 calculated on the assumption of no buildup. From this we conclude that no significant buildup (within experimental error) of the incident shock front occurred in the first 80% of run to detonation. It is also evident in Figs. 7 and 8 that the rate of the pressure excursions--again identified with decomposition of the explosive--following these wave arrivals tends to increase with increasing R.

For the two experiments with $R > 0.8$ (7-3 and 7-9, both shown in Fig. 7), the observed P_2 is significantly larger than P_2, corresponding to some buildup of the shock front. It is not determined

whether the onset of relatively fast and complete reaction of the explosive results in some real fluid-dynamic behavior being responsible for the pressure minimum and subsequent rise observed in the profiles, or whether the signal is just some fairly reproducible mode of gauge failure induced by very high pressures.

D. Effect of Reflected Waves

Some consideration was given to the possibility that the reaction producing the pressure excursions observed at the target gauges was due to the higher pressures produced in the samples by the wave reflected from the quartz element, and thus was not representative of the pressure histories that would occur if a single shock were to continue to propagate. To examine this question, a pair of experiments, 7-10 and 7-11, were performed with 0.82-mm Lucite "buffer" layers between the PETN and the target gauge. The buffer was thin enough that a shock reflected from the gauge element could interact with the PETN during the time of the measurement, but thick enough to insure that the interaction did not affect the first 0.45 μsec of the gauge signal. The buffer material has a slightly "softer" Hugoniot than 1.7-g/cm^3 PETN, so the passage of the shock across the explosive-Lucite interface generated a rarefaction that was propagated back toward the projectile gauge.

A comparison of target-gauge profiles from experiments with and without buffer layers is given in Fig. 9. With the Lucite layer, the back-face pressure increase occurs before any reflected shock reaches the explosive, and continues to increase smoothly, in a fashion quite similar to that of the comparable shot without the buffer. The same behavior was seen in Shot 7-11. These shots demonstrate that the reaction induced by the reflected waves is not primarily responsible for the form of the target-gauge pressure profiles, but there is still the possibility that the reflected shock does increase the decomposition rate to some small degree.

The projectile-gauge profiles in Fig. 9 are also of interest. The profile for Shot 7-7 is typical of the experiments on thinner samples, where the arrival on the reflected shock is observed,* and

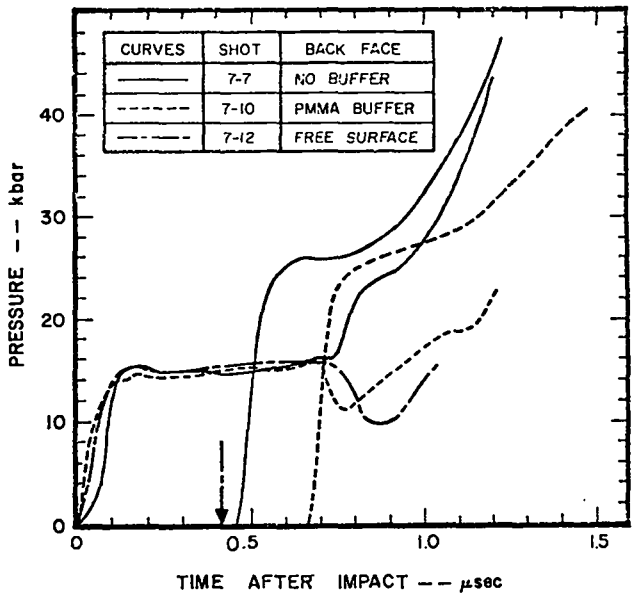

Fig. 9. Comparisons of pressure profiles from shots with and without a Lucite buffer, and with a free surface at the back interface. The arrow indicates the shock arrival time at the free surface in Shot 7-12, as measured with a ferroelectric pin.

appears to be superimposed on the pressure excursion characteristic of the profile for thicker samples. Similarly, the rarefaction wave in Shot 7-10 arrives at the proper time and causes a pressure dip, but does not suppress a subsequent pressure excursion. Most informative is the similar profile obtained in Shot 7-12, where the back sample interface was with a vacuum. In an inert with shock properties like PETN, the arrival of the rarefaction wave would be expected to cause cavitation at the projectile gauge-sample interface, and a zero gauge signal, but again the pressure excursion appears. These observations strongly suggest that the reaction providing the impact-face pressure excursions is induced by the initial shock and that the subsequent course of the decomposition is affected relatively little by the pressure in the explosive.

E. Observations on 1.6-g/cm^3 PETN

Only five successful experiments were performed on PETN pressings of nominal 1.6-g/cm^3 density, and these were not ideally chosen for input shock strength and sample thickness.

The description of the results of these shots is limited to the examination of a pair of typical observations (Fig. 10) and some comparisons of the

*Note, however, that this second reflected-shock pressure is not greater than the initial target-gauge pressure, P_2, as would be expected in an inert.

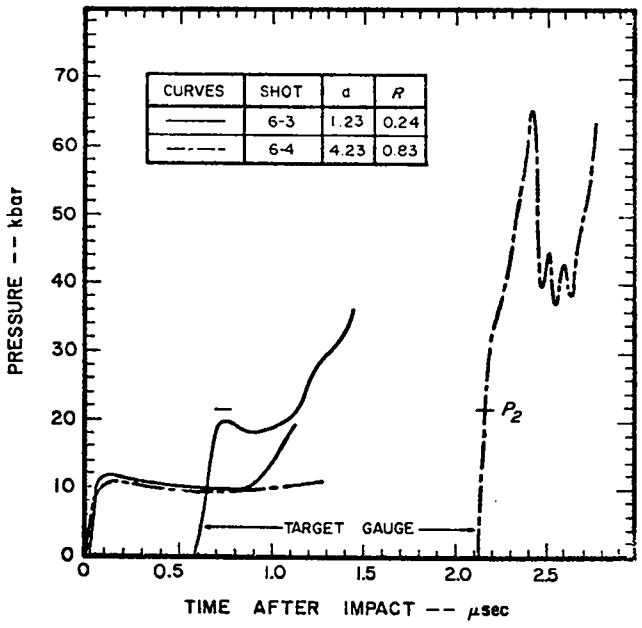

Fig. 10. Pressure profiles obtained with nominal 1.6-g/cm^3 pressings. Initial shock pressures in both shots were about 10 kbar, corresponding to about 5.1-mm distance to detonation. The pressure rise on the projectile-gauge record for Shot 6-3 is a reflected shock, and not induced by decomposition.

observations with those for the higher density PETN. As can be seen in Table III, the shots on the lower density samples were done mostly with input shock pressures about two-thirds those used with the 1.7-g/cm^3, but yielded vary comparable distances to detonation. Projectile-gauge records for the 1.6-g/cm^3 explosive generally displayed an initial relaxation in pressure of about the same magnitude as for the higher density pressings, but requiring about twice the time. In the three experiments with samples thick enough to have impact-face records uninfluenced by reflected waves, no significant pressure excursions were observed.

The target-gauge profiles for the lower density explosive were essentially of the same two types as observed for the 1.7-g/cm^3 pressings, and had a similar correlation to the parameter R. Examination of Table III reveals that the onset of significant increase in shock-front pressure must begin at a smaller fraction of the run to detonation; the selection of experiments did little to establish a critical value of R, determining only that it is greater than 0.33 and less than 0.76.

F. Comparison of Observations in Front-Back and Wedge-Shot Experiments

In addition to the Hugoniot data and buildup parameters used earlier, the explosive wedge experiments on high-density PETN[13] have other features that are quite consistent with the observations in this work. In the wedge shots on 1.72-g/cm^3 PETN, no acceleration of the shock front was seen over nearly the entire run to detonation. Thus, the quartz-gauge observation that the shock-front pressures in 1.7-g/cm^3 PETN have no significant increase for 80% of the estimated run to detonation should come as no great surprise. Similarly, the wedge studies on 1.6-g/cm^3 PETN did display discernible shock-front acceleration during the last half of the run to detonation, consistent with the observations in this work that pressure buildup at the front begins at some lower value of R in the 1.6-g/cm^3 pressings.

The idea of a "second-wave phenomenon" in 1.72-g/cm^3 PETN arose from the observation of a disturbed region on the face of the wedges behind the shock front (see Fig. 2 in Ref. 13). This feature was identified as an increase of the velocity of the wedge's free surface. Typically it became visible about a half-millimeter into the wedge and about a half-microsecond after the shock had entered, and it appeared to advance toward the leading shock front. The disturbed region was of some width, more or less bounded by lines that corresponded to the trajectories of waves propagating at about 6 and 9 mm/μsec. Invariably, the abrupt acceleration of the front to detonation velocity--about 8 mm/μsec --occurred when the converging fan of disturbed area "overtook" the leading shock. We concluded that the disturbance began in the interior of the sample with decomposition which generated a pressure wave that overtook the front and effected detonation.

The same conclusion can be developed from the front-back experiments. When one knows the initial sample thickness, the gauge pressure as a function of time, and when the appropriate quartz Hugoniot is used to determine the interface velocity,* the position of each sample-gauge interface can be calculated as a function of time. Thus the interface position-time coordinates which correspond to a

*This method will be described in more detail in the following section.

given pressure can be determined, and data can be combined for shots with different sample thicknesses. This was done for Shots 7-7, -8, and -9 (see Fig. 8), for target-gauge pressures of 1.0, 1.25, 1.5, and 2.0 times the nominal initial reflected-shock strength of an incident wave without buildup. Pressure information from the impact face was included by determining points from the projectile-gauge data with the same ratios applied to the nominal initial shock strength of 15 kbar.

The constant-pressure loci resulting from the calculation are plotted in Fig. 11, where the curve for a unity pressure ratio essentially represents the progress of the leading shock front. The distance-time domain of the pressure disturbance in the front-back experiments is totally similar to the field of the free-surface-velocity disturbance in a typical wedge experiment. The converging set of constant-pressure contours corresponds to a compressive wave that grows steeper with run. It is only when this wave overtakes the leading shock front that the relatively abrupt onset of detonation occurs. The quartz-gauge measurements thus corroborate the existence and role of the "second wave" deduced from the wedge-shot observations. We argue that this wave originates from decomposition in the interior of the shocked explosive because no other means of generating it was present in the experiment.

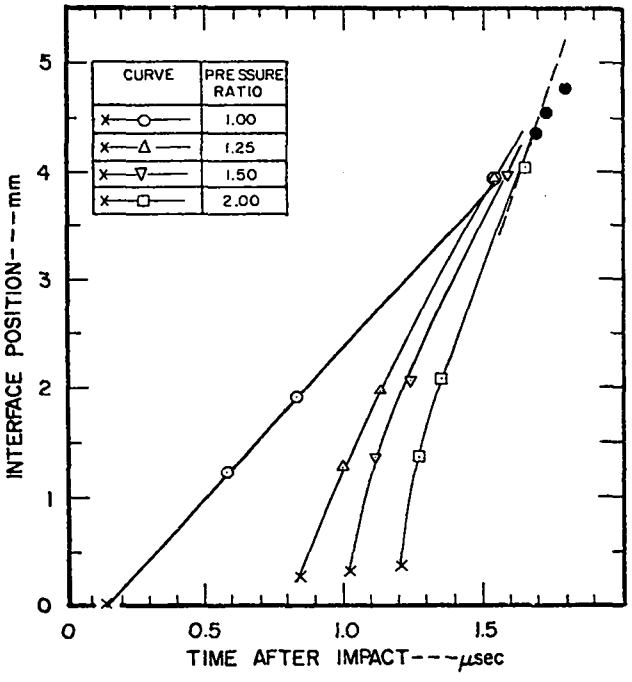

Fig. 11. Position and times of constant pressure ratios observed in Shots 7-7, -8, and -9. The open symbols represent determinations from the target-gauge measurements, the X's are projectile-gauge data, and the solid symbols show the expected times and distances to detonation for the three experiments. The solid symbols have been plotted with an 0.14-usec time adjustment for gauge signal risetime. The dashed line is for reference, and has a slope of 8 mm/μsec, corresponding to detonation velocity.

IV. ESTIMATES OF WAVE STRUCTURES AND DECOMPOSITION

Like most techniques for studying shock initiation, front-back experiments provide information on the reacting explosive only at its interface with an inert, and do not provide direct measures of the pressures and decomposition in the interior of the sample. Any development of pressure-distance and decomposition-distance profiles requires some assumptions and considerable calculation. One method used for such development is to model some reaction-rate "law" into a one-dimensional numerical hydrodynamic treatment of the experiment, and to vary parameters until the calculated behavior at the interface simulates the observations. Such computations may provide some argument for the reality of both the assumed rate law and the calculated pressure and reaction fields. Jacobson and Fickett have performed such a calculation[28] for the data of Shots 7-7, -8, and -9, with good results. These calculations will be discussed later, following a more detailed description of our development of decomposition estimates from the same data, using a more direct method.

A. The Direct Analysis Method

Given the temporal behavior of the pressure (or velocity) field in a reacting explosive and a complete equation of state for the reactant-product mixture, the decomposition history of the material can be calculated by a direct analysis. Starting with the pressure field, the particle-velocity, density, and energy fields are successively determined by integration of the fluid-dynamic conservation laws. These determinations, the equation of state, and the laws of thermodynamics are then used to obtain the energy release and decomposition. Such an analysis method was recently described by

Cowperthwaite.[29] Our method appears somewhat different from Cowperthwaite's, particularly in that we do not use the "phase velocities" of Fowles and Williams,[30] but in this respect the two methods are actually equivalent.[31]

The governing equations for our analysis are those of mass, momentum, and energy conservation, plus a thermodynamic relation between the rates of change in pressure and density and the reaction rate. In the appropriate Lagrangian form, the first three relations are

$$\rho_o \frac{\partial v}{\partial t} - \frac{\partial u}{\partial h} = 0 \quad ,$$

$$\rho_o \frac{\partial u}{\partial t} + \frac{\partial P}{\partial h} = 0 \quad ,$$

and

$$\frac{\partial E}{\partial t} + P\frac{dv}{dt} = 0 \quad ,$$

where t and h are the independent time and space coordinates, $v = (1/\rho)$ the specific volume, and ρ_o the initial density. For our analysis, we have chosen the thermodynamic relation of Kirkwood and Wood:[32]

$$\frac{1}{\rho c^2}\frac{\partial P}{\partial t} - \frac{1}{\rho}\frac{\partial \rho}{\partial t} = \sigma \frac{\partial \lambda}{\partial t} \quad ,$$

where λ is the degree of reaction, ranging from 0 for the unreacted solid to 1 for complete decomposition. In general, both the frozen sound speed, c, and the heat release parameter, σ, must be determined from a complete P-v-E-λ equation of state.

The first step in our direct analysis is to construct the pressure fields, $P(h,t)$, at different times, by interpolating between the data obtained at fixed space coordinates as a function of time. Pressure gradients occurring after shock arrival are then evaluated at several space coordinates as a function of time, and the momentum equation is integrated to yield the particle velocity. This can be expressed formally as:

$$u_j = u_{j,1} - \frac{1}{\rho_o}\int_{t_1}^{t} \left(\frac{\partial P}{\partial h}\right)_j dt \quad ,$$

where the sub-j indicates values along a particle path and the sub-1 indicates the value of the parameter at shock arrival. Having established the particle-velocity fields, velocity gradients are determined for several h_j and the density fields are obtained by integration of the continuity equation:

$$\frac{1}{\rho_j} = \frac{1}{\rho_{j,1}} + \frac{1}{\rho_o}\int_{t_1}^{t} \left(\frac{\partial u}{\partial h}\right)_j dt \quad .$$

Time derivatives of the density are also determined from the continuity equation:

$$\left(\frac{\partial \rho}{\partial t}\right)_j = -\frac{\rho_j^2}{\rho_o}\left(\frac{\partial u}{\partial h}\right)_j \quad ,$$

and $(\partial P/\partial t)_j$ is evaluated directly from the pressure-field construction.

Next, c and σ must be determined from the assumed equation of state and the calculated state variables. In general, this requires specification of E and λ as well as the already-determined P and ρ. The internal energy fields are obtained by integrating the conservation relation:

$$E_j = E_{j,1} + \int_{t_1}^{t} P_j \left(\frac{\partial v}{\partial t}\right)_j dt = E_{j,1} + \int_{t_1}^{t} P_j \left(\frac{\partial u}{\partial h}\right)_j dt \quad .$$

Determination of λ requires that the entire analysis be conducted by a stepping-ahead procedure, starting at $t = t_1$ and $\lambda = 0$. At each step, the reaction rate is calculated from the Kirkwood-Wood relation, and the decomposition field is updated by integrating the rate.

In the example discussed below, we used a simplifying assumption that made c and σ functions of pressure alone. Thus, calculation of the internal energy and the stepping-ahead procedure were unnecessary.

B. Assumptions, Approximations, and Calculation of the Example

The results of Shots 7-7, -8, and -9, yielding pressure-time profiles at h = 0, 1.22, 1.92, and 3.95 mm, were the subject of our direct analysis. These data (see Fig. 8) were adjusted to the same initial density and input shock conditions, with the latter parameters calculated from the projectile velocity and the quartz and PETN Hugoniots described in Sec. II. We consider that a semi-infinite, homogeneous, 1.7-g/cm^3 PETN sample is impacted with a quartz warhead moving 0.44 mm/μsec. The pressure initially generated in the explosive is 16.5 kbar and the particle and shock velocities are, respectively, 0.33 and 2.94 mm/μsec. The shocked density is 1.915 g/cm^3, the "bulk" temperature 370°K, and the sound speed is 3.41 mm/μsec. The expected distance and time to detonation are 4.62 mm and 1.62 μsec. We deduct 0.14 μsec risetime from the projectile-gauge record of Shot 7-9, and treat the first 0.45 μsec of the profile as constant, and let the impact-face pressure increase thereafter according to the recorded gauge pressure. Arbitrary extrapolations of the gauge data were made as needed to extend the measurement time to 1.35 μsec after impact.

The principal assumptions, approximations, and additional input used in the calculation were:

(a) The pressure histories at interior points of the semi-infinite sample were assumed to be related to the reflected-wave pressures observed at the corresponding PETN-target gauge interfaces by the standard impedance-match solution. The manner of this determination is illustrated in Fig. 5, where P_r represents the target-gauge observation and P_b is the corresponding pressure in the semi-infinite sample. The impedance-match solution was calculated with the quartz Hugoniot and PETN equation of state given in Sec. II, and it was found that the proportionality

$$P_b = 0.606\ P_r$$

fit the solution to within 1% over the pressure range of the data.

This assumption is the weakest of our entire analysis, and has three debatable implications. First, P_r is calculated along the single-shock Hugoniot. As long as the actual process is along a compression isentrope (as it would be for inerts) approximation of the P - ρ state with the Hugoniot usually does not produce serious error. However, as reaction occurs the material state must deviate from the isentrope, and substantial error may be introduced as the decomposition becomes extensive. A second implication of this assumption is that the increased pressure from the reflected wave does not alter the decomposition process; some justification for this premise was given in Sec. III. Finally, even if the target gauge did not introduce a reflected shock, there is no argument to support the assumed equivalence of behavior at an explosive-inert interface with that of an embedded mass point with reacting material on both sides.

(b) A zero pressure gradient at the shock front was assumed for the first 80% of the run to detonation. Justification for this assumption is inferred from the observed lack of buildup at the shock front and the shock-change equation.[33] This equation is:

$$\left(\frac{dP}{dh}\right)_S = \frac{\rho_o\,(U-u)\sigma\,(\partial\lambda/\partial t)_S - (1-M^2)\,(\partial P/\partial h)_S}{M^2 + [\rho_o U/(dP/du)_H]}$$

where $(dP/dh)_S$ is the pressure change at the shock front as it moves, the sub-S indicates that the partial derivatives are evaluated at the shock front, the sub-H denotes the derivative along the Hugoniot. The Mach number, $M = (U-u)/c$, is required to be less than unity by our equation of state. According to the equation, zero pressure change with shock run thus requires: a positive pressure gradient with exothermic reaction (more specifically, a positive σ), or endothermic reaction with a negative pressure gradient, or that both the gradient and reaction vanish at the front. Our observations provide no evidence of a positive pressure gradient, and endothermic reaction seems implausible; thus, we have chosen the third alternative.

(c) The continuity of pressure and particle velocity across a contact surface and the quartz Hugoniot was used to calculate the impact-face

particle velocity. This simplification is not an assumption, but rather embodies the approximation of equating the compression isentrope for quartz with its Hugoniot, which introduces trivial error. The path P_1, u_1 to P_i, u_i in Fig. 5 illustrates the relation of impact-face particle velocity to the projectile-gauge pressure.

(d) The PETN state was considered to always be near the Hugoniot, and the values of ρc^2 and σ used were calculated along this locus. This approximation makes ρc^2 and σ functions of pressure alone, and permits the calculation of c from the equation of state specified in Sec. II. The heat release parameter was determined from the relation:[32]

$$\sigma = -\frac{\Delta_r \rho}{\rho} - \frac{\Gamma \Delta_r H}{c^2}$$

where Δ_r denotes the partial derivative with respect to λ at constant pressure and temperature and H is the specific enthalpy. To evaluate σ, the heat of decomposition, $-\Delta_r H$, was assumed independent of P and λ, and equal to 62.7 kbar-cm^3/g.[34] In estimating $\Delta_r \rho$, the decomposition of PETN was considered as:*

$$C(CH_2ONO_2)_4 \rightarrow 4H_2O + 4CO_2 + C + 2N_2 \quad .$$

Hugoniot data on the condensed phase of each reaction product[35,37] provided estimates of their densities at appropriate pressures, and ideal mixing was assumed to obtain the overall reaction-product densities. The calculated relations of $\Delta_r \rho/\rho$, σ and ρc^2 to shock pressure are shown in Fig. 12.

Simple graphical methods were used to follow the analysis procedure described earlier. Profiles

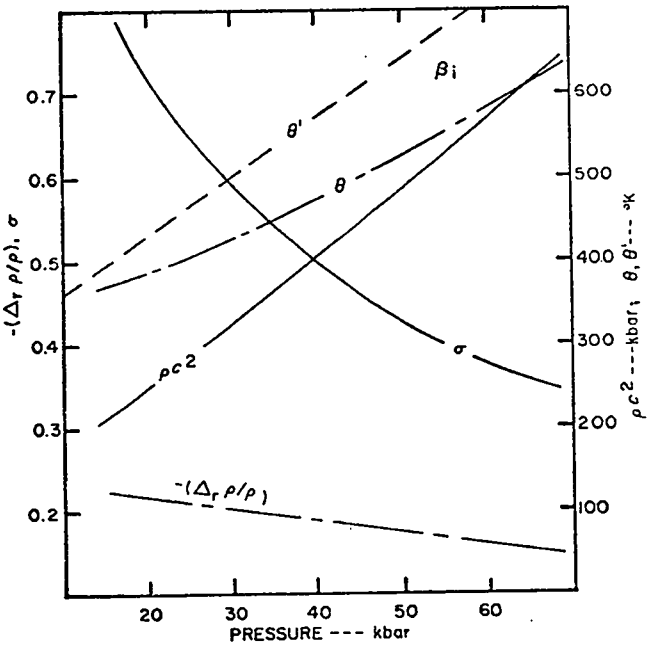

Fig. 12. Equation-of-state variables on the shock Hugoniot for 1.7-g/cm^3 PETN. The "bulk" shock temperatures, θ and θ', are calculated as described in Sec. II and by the simplified Grüneisen form of Jacobson and Fickett, respectively. As discussed in Ref. 13, these temperatures are far too low to effect the prompt initiation of PETN. In the usual Arrhenius rate expression (Ref. 38), the rates obtained are orders of magnitude below those of our calculated example.

obtained at various stages of the analysis are shown in Figs. 13-a through -d and Fig. 14-a. Discussion of these results will be deferred until the numerical hydro calculation of the same example is described.

C. Numerical Hydro Calculation of the Example

Jacobson and Fickett have calculated our example with a one-dimensional numerical hydrocode, using the same average initial conditions as we did for Shots 7-7, -8, and -9. Their PETN solid equation of state was essentially that given in Sec. II. The gaseous reaction products were represented by a polytropic gas equation of state, with a ratio of specific heats of 2.9. Mixing of the solid and gas phases was accomplished with a partial pressure scheme.

A first order Arrhenius form was used for the rate law:

$$\frac{\partial \lambda}{\partial t} = Z\,(1 - \lambda)\, e^{-\theta^*/\theta'} \quad .$$

---

*This formulation of the reaction is approximately that calculated in Ref. 35 for the "CJ composition" of reaction products from the detonation of high-density PETN. We consider it more appropriate for the densities and temperatures of our example than:

$$C(CH_2ONO_2)_4 \rightarrow 4H_2O + 3CO_2 + 2CO + 2N_2 \quad ,$$

as cited elsewhere.[34,36] Use of the latter decomposition scheme increases σ by about 10%.

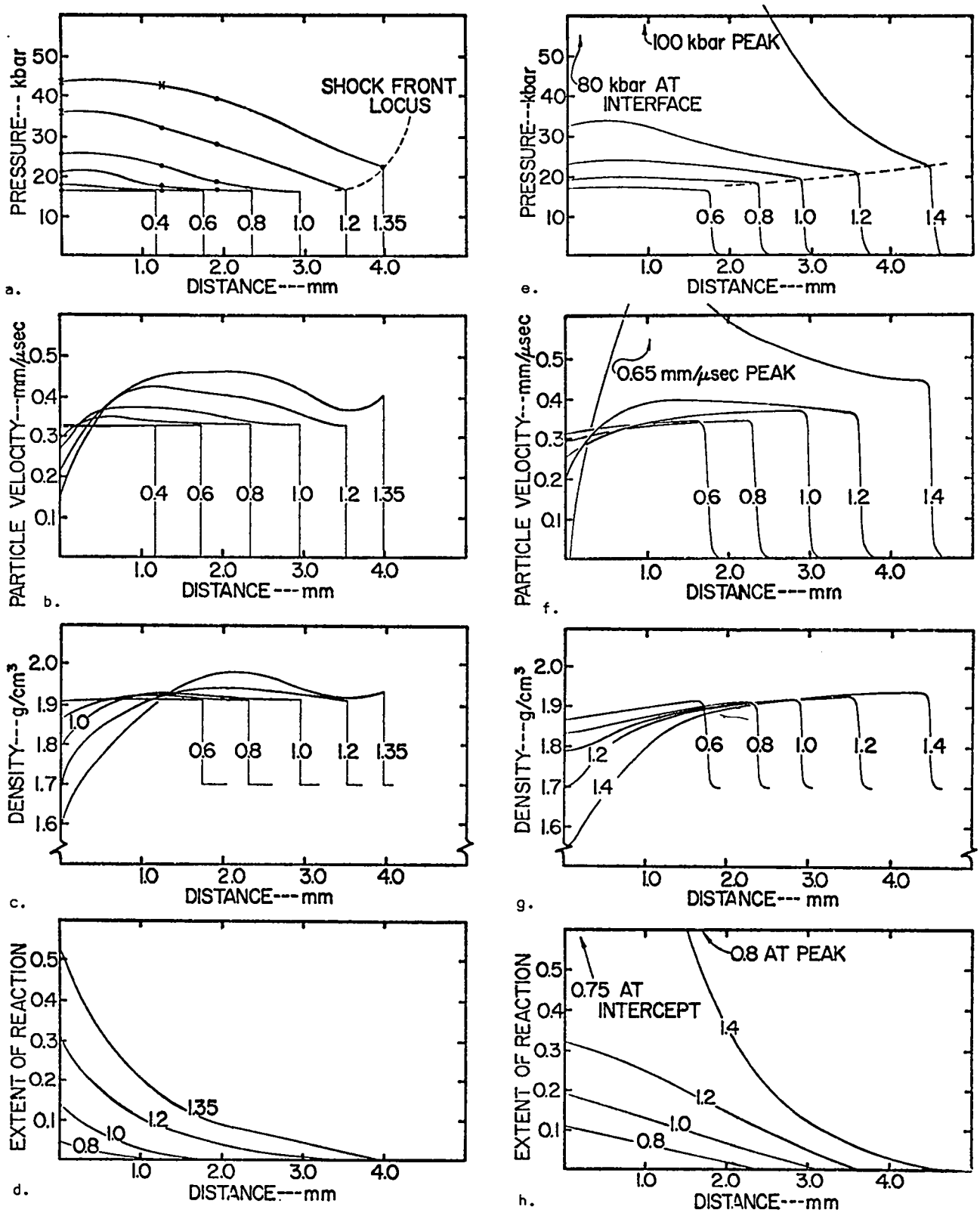

Fig. 13. Calculated pressure, particle-velocity, density and decomposition profiles for Shots 7-7, -8, and -9. The left-hand profiles were obtained by direct analysis and the numerical hydro calculations of Jacobson and Fickett gave those shown on the right. The numbers labeling each curve give the time after impact in microseconds. The solid dots in frame a. represent the quartz-gauge measurements, and the x's are extrapolations of the gauge data.

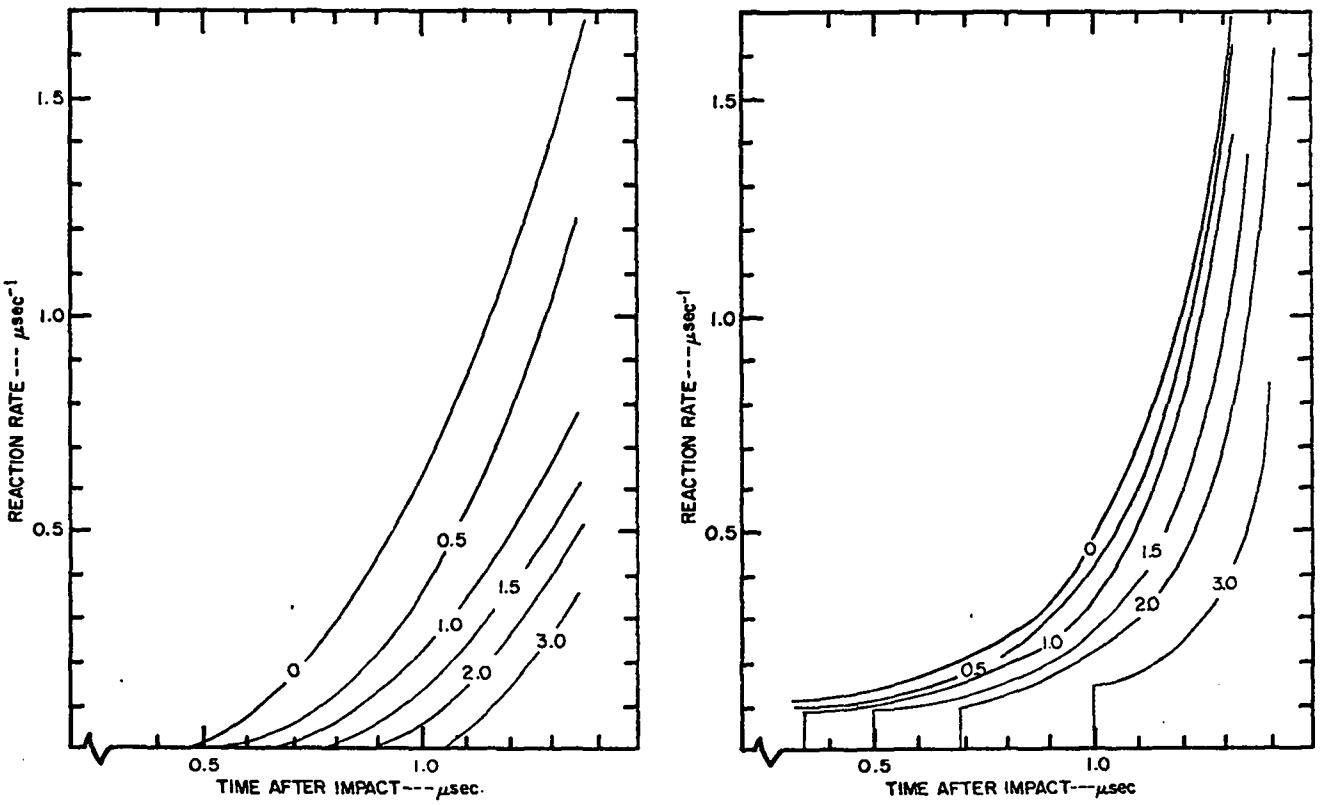

Fig. 14. Calculated reaction-rate profiles for Shots 7-7, -8, and -9. Again, profiles from the direct analysis are on the left. Rates from Jacobson and Fickett's computation, on the right, were determined by using their calculated values of temperatures and reaction extent in the rate law given in the text. The labels on each curve indicate the distance from the impact face in millimeters.

Z = 150 μsec^{-1} and θ^* = 3000°K were chosen to force agreement with experiment.* The temperature, θ', was calculated with a simplified "Grüneisen" form:

$$\theta' = 300 + 7P + 11.5\,(P - P_H)\ , \quad (^\circ K;\ P,\ P_H \text{ in kbar})$$

where P and P_H are, respectively, the mixture pressure and pressure along the solid Hugoniot at the appropriate specific volume. This formulation gives an acceptable detonation temperature,[35] but--as seen in Fig. 12--gives Hugoniot temperatures ~100°K higher than the calculation of Sec. II in the 20- to 70-kbar pressure region of our example.

*Thermal initiation experiments cited in Ref. 38 give $Z = 6.3 \times 10^{13}$ μsec^{-1} and θ^* = 24,000°K. The arbitrary parameters of Jacobson and Fickett give rates much less sensitive to temperature and an unrealistic rate at room temperature. Both sets of coefficients yield the same 3.3-μsec^{-1} rate at 785°K.

Results of the numerical hydro calculation are shown in Figs. 13-e through -h and Fig. 14-b. Good agreement with observation is seen in the pressure profiles. Slightly large, but reasonable, values for the time and distance to detonation were obtained. The profiles generally are in agreement with those from the direct analysis at times and positions where data were actually obtained. The differences in the calculations at later times could have been reduced if steeper extrapolations of the pressure-time profiles had been used in the direct analysis.

For the time range covered by data, the numerical hydro calculation differs from observation primarily in predicting a modest buildup of the shock front during the first part of its run and an increase of the impact-face pressure commencing at time zero. Constraints commensurate with nonincreasing impact-face and shock pressures were imposed in the direct analysis. This produced

"induction times" for the start of reaction, in contrast with the results of the numerical hydro analysis. As will be discussed later, the observed impact-face and shock-front pressure behavior could be due to a relaxation phenomenon unrelated or incidental to the decomposition process. The addition of some compensation for pressure relaxation to the present reaction model in the hydro calculation would improve its agreement with observation. Similarly, inclusion of a relaxation term in the Kirkwood-Wood relation of the direct analysis could alter the obtained extents of reaction and reaction rates to more nearly resemble those obtained by Jacobson and Fickett.

V. DISCUSSION

A. Some Conclusions and Comparisons from the Example

Although numerous approximations were used in the analyses described in the previous section, Figs. 13 and 14 provide at least a qualitative picture of the initiation behavior in the chosen example. Both calculations show that decomposition begins near the impact face. Jacobson and Fickett's calculation shows complete reaction near the impact face in less than 1.5 μsec, and reasonable extrapolation of the direct analysis gives complete impact-face decomposition slightly before the 1.62-μsec time to detonation. The reaction rates build to moderate values (compared with 20 to 50 μsec^{-1} in a detonation wave in PETN), producing a pressure wave that advances on the shock front. The shock front itself has little or no buildup until it is overtaken by the pressure wave, after which the transition to detonation is relatively abrupt. Particularly with the numerical hydro treatment, the initiation behavior resembles that considered typical of homogeneous explosives.

The pressure profiles from both calculations resemble those attributed to Dremin as occurring in the early stages of the buildup of pressed TNT,[39] as based on his measurements of particle velocity with a magnetic probe.[8] Dremin's construction differs from our picture in that the initial shock strengths represent a larger fraction of the eventual detonation pressure (appropriate for the less sensitive explosive), and the buildup of the shock front pressure and the onset of detonation is a more gradual process.

Craig and Marshall have performed free surface velocity measurements[10] and Kennedy has obtained pressure-gauge measurements[11,12] on PBX-9404 with shock conditions yielding initiation distances comparable to that of our example. The comparison of our results with the waveforms inferred from these experiments is particularly interesting.

Mader was able to simulate Craig and Marshall's observations with reactive numerical hydro calculations.[40] With the knowledge[41] that a relatively gradual (compared with PETN) "single-curve buildup"[3,4] typifies the shock initiation of 9404, and from observations of the early development of a pressure spike at the front,[10] Mader chose to completely separate the reaction model producing the front buildup from a "Dremin burn" which provides delayed energy release in the interior of the sample. The resulting calculated wave structures differ substantially from ours near the shock front. The pressure-distance profiles in the region of Dremin burn slightly resemble those of Fig. 13 and, with proper adjustment of constants, the empirical formulation of this rate mechanism probably could be made to reproduce the results on PETN quite adequately.

Recently Kennedy has supplemented his front-back experiments[11] on 9404 with manganin gauge measurements of pressure profiles, and has used these higher pressure data in deducing wave structures.[12] For the first half of the run to detonation, his constructions closely resemble those of Fig. 13. He believes that a pressure hump develops near the shock front after about half of the run to detonation, and provides the principal contribution to its buildup. Accepted unequivocally, target-gauge records as in Shot 7-9 would indicate a similar behavior in 1.7-g/cm^3 PETN, but with the pressure hump occurring relatively late in the buildup. Although our data are too sparse to demonstrate it, the initiation behavior of 1.6-g/cm^3 PETN might be a much better analog to Kennedy's picture of the wave structures in 9404.

Jacobson and Fickett carried their numerical hydro calculation of our example through the time of detonation, and the direct analysis and wedge-shot observations can also be examined to infer the nature of the late stage of the buildup. Different behaviors are implied by the two treatments.

The relatively large amplitude of the following wave developed in Jacobson and Fickett's calculation produces the abrupt and drastic change of shock-front pressure to account for its prompt buildup to detonation. The whole process is satisfactorily treated with the single rate law, suggesting that a single mechanism dominates the buildup.

The direct analysis leads to a more complicated interpretation. At late times, the calculated pressure gradients are insufficient to account for the rate of shock-front buildup, and relatively fast reaction must start at the front, more or less spontaneously. For example, use of the pressure change and gradient at 1.35 μsec (see Fig. 13-a) in the shock-change equation gives a reaction rate of ∿0.9 μsec^{-1} at the front, while immediately behind the front, rates are much lower (see Fig. 14-a). It might be argued that this higher rate is merely that characteristic of the enhanced shock strength at 1.35 μsec (∿23 kbar, as opposed to the 16.5-kbar initial shock strength). If so, one might expect a wedge experiment with a 23-kbar input to build to detonation in the 0.27-μsec time remaining to detonation in our example. As formulated in Sec. II, a 23-kbar input corresponds to a time to detonation of 0.83 μsec. This all suggests that a second mechanism effects the final buildup at the front.

With our present data, we would more readily accept the simpler late-stage behavior calculated by Jacobson and Fickett. As remarked before, the differences in the two analyses arise from the modest pressure changes in the early stages of the example and from differences in extrapolations at later times. We believe the early-time discrepancies can be eliminated by the proper accounting of stress relaxation effects; resolving the validity of the extrapolations will require more measurements using higher pressure diagnostics than we have obtained with quartz gauges.

B. Pressure Relaxation Effect

A 1- to 2-kbar pressure relaxation was consistently observed in our projectile-gauge records. It seems likely that the process causing this effect at the impact face would also alter the pressure immediately behind the shock wave. A complicated competition of some relaxation process with mechanisms that would contribute to the shock buildup, such as overtaking pressure waves and reaction, may well be responsible for the shock-front pressure remaining essentially constant for so much of its distance of run to detonation. Possible causes of the pressure relaxation are sluggish phase transitions involving sufficient densification or energy absorption, an initial endothermic stage to the reaction, and the delayed collapse of voids in the pressing.

There is no known phase transition in PETN that could be a source of the pressure relaxation. Isothermal, static compression data to 20 kbar give no indication of a polymorphic transition at room temperature.[42] A disordered phase of PETN does exist,[43] but it has been produced only in special crystallization processes[44] and is not likely to result from shock compression; furthermore, the modest enthalpy increase and the positive specific volume change of the transition would lead to an increase, rather than a decrease, in observed pressure. The calculated "bulk temperatures" at our typical shock strengths are below that for melting PETN (∿140°C at atmospheric pressure), but certainly a portion of explosive is heated beyond the melting temperature. The heat of fusion of PETN, about 1.5 $kbar\text{-}cm^3/g$,[44] would be sufficient for the observed pressure relaxation if the melting were extensive and if it were a constant-volume process. Direct measurements of this volume change of melting are not known, but measurements of the pressure-temperature phase line[45] and the Clayperon-Classius relation indicate about a 9% volume increase on melting. Again, the melting transition would not lead to a pressure decrease.

Craig has suggested that the pressure relaxation could manifest an initial endothermic stage of the reaction,[41] and in the absence of knowledge of the decomposition kinetics of PETN this explanation must be a possibility. The accepted activation energy for PETN reaction (6.2 $kbar\text{-}cm^3/g$)[38] is ample to be consistent with such a premise.

In an additional front-back shot, we observed a similar impact-face pressure relaxation in a comparable experiment on an inert mockup (1.7-g/cm^3 pressed ammonium sulfate) of PETN. This has led us to believe that some mechanical property generic to pressed solids, rather than a unique property of PETN, is responsible for the relaxation. We propose a relatively slow void collapse as the source of the phenomenon. If some residual void fraction after

the initial shock is assumed, and the bulk sound speed is used to estimate the density change associated with a pressure decrease, then, for example, a 1% reduction in void fraction would result in a 1.2-kbar pressure change. Suitably large residual void fractions in shocked material that had initial porosities of 4 to 5% seem quite plausible.

For our pressings, void dimensions would probably be of the order of 0.01 mm and, if closed with material moving at the free-surface velocities typical of our experiments, collapse would occur in times an order of magnitude less than our observations show. However, if a sensible shear strength is ascribed to the matrix material, the collapse process is much slower,[46] so that the ∿0.5-μsec relaxation times we see are reasonable. Taylor and Christianson have extended this model, noting that the shear work on the solid material concentrated at the void periphery would be converted almost entirely into heating the explosive, thus inducing its reaction.[46] We believe this process is a likely candidate for the hot-spot mechanism causing the initiation of high-density PETN, and deserves further theoretical examination.

ACKNOWLEDGMENTS

As well as lending their gas gun to the investigation, Charles W. Caldwell, Joseph N. Fritz, John W. Hopson, and John W. Taylor of Los Alamos Scientific Laboratory Group M-6 generously provided help in conducting the experiments and analyses. Among those in Group WX-7 aiding in the program were Melvin G. Duran, Frank Vaughn, and Donald L. Wilson, and S. D. Gardner provided a critical review of the manuscript. We also appreciate the useful discussions with Wildon Fickett and Jack Jacobson of Group T-4, with Robert A. Graham and James E. Kennedy of Sandia Laboratories, and with Michael Cowperthwaite and D. R. Curran of Stanford Research Institute.

REFERENCES

1. A. W. Campbell, W. C. Davis, J. B. Ramsay, and J. R. Travis, "Shock Initiation of Solid Explosives," Phys. Fluids 4, 511 (1961).

2. G. E. Seay and L. B. Seely, Jr., "Initiation of a Low-Density PETN Pressing by a Plane Shock Wave," J. Appl. Phys. 32, 1092 (1961).

3. I. E. Lindstrom, "Plane Shock Initiation of an RDX Plastic-Bonded Explosive," J. Appl. Phys. 37, 4873 (1966).

4. I. E. Lindstrom, "Planar Shock Initiation of Porous Tetryl," J. Appl. Phys. 41, 337 (1970).

5. S. J. Jacobs, T. P. Liddiard, Jr., and B. E. Drimmer, "The Shock-to-Detonation Transition in Solid Explosives," in Ninth Symposium (International) on Combustion (Academic Press, New York, 1963), p. 517.

6. H. Bernier, J. M. Lezaud, and Y. Chevalier, "Étude Expérimentale et Théorique de la Génération de la Détonation par Onde de Choc Dans un Explosif Granulaire," in Behavior of Dense Media Under High Dynamic Pressures (Gordon and Breach, New York, 1968), p. 51.

7. A. W. Campbell, W. C. Davis, and J. R. Travis, "Shock Initiation of Detonation in Liquid Explosives," Phys. Fluids 4, 498 (1961).

8. A. N. Dremin, and S. A. Koldunov, "Initiation of Detonation by Shock Waves in Cast and Pressed TNT," Vzryvnoye delo 63, 37 (1967). English translation in UCRL-Trans-10408.

9. Julius Roth, "Shock Sensitivity and Shock Hugoniots of High-Density Granular Explosives," in Fifth Symposium (International) on Detonation, Office of Naval Research report ACR-184, p. 219.

10. B. G. Craig, and E. F. Marshall, "Decomposition of a Solid Explosive when Shocked but not Detonated," ibid., p. 321.

11. J. E. Kennedy, "Quartz Gauge Study of Upstream Reaction in a Shocked Explosive," ibid., p. 435.

12. J. E. Kennedy, "Pressure Field in a Shock-Compressed High Explosive," in 14th Symposium (International) on Combustion, (The Combustion Institute, Pittsburgh, 1973), p. 1251.

13. Dante Stirpe, James O. Johnson, and Jerry Wackerle, "Shock Initiation of XTX-8003 and Pressed PETN," J. Appl. Phys. 41, 3884 (1970).

14. G. E. Ingram, and R. A. Graham, "Quartz Gauge Technique for Impact Experiments," in Fifth Symposium (International) on Detonation, Office of Naval Research report ACR-184, p. 369.

15. R. J. Wasley, and F. E. Walker, "Dynamic Compressive Behavior of a Strain-Rate Sensitive, Polycrystalline, Organic Solid," J. Appl. Phys. 40, 2639 (1969).

16. R. A. Graham, F. W. Neilson, and W. B. Benedick, "Piezoelectric Current from Shock Loaded Quartz - A Submicrosecond Stress Gauge," J. Appl. Phys. 36, 1775 (1965).

17. O. E. Jones, "Piezoelectric and Mechanical Behavior of X-Cut Quartz Shock Loaded at 79°K," Rev. Sci. Instr. 38, 253 (1967).

18. R. P. Reed, "The Sandia Field Test Gage, Its Characteristics and Data Reduction," Presented at the Underground Nuclear Test Measurements Symposium I, Preprint, Sandia Laboratories report SC-DC-71 4529 (1972).

19. P. E. Taylor, "A New Electrode Configuration for Thick Quartz Pressure Gauges," presented at the Underground Nuclear Test Measurements Symposium I, (Sandia Laboratories, December, 1971).

20. Jerry Wackerle, "Shock-Wave Compression of Quartz," J. Appl. Phys. 33, 922 (1962).

21. R. A. Graham, and G. E. Ingram, "Piezoelectric Current from X-Cut Quartz Shock-Loaded from 25 to 70 kbar," Bull. Am. Phys. Soc. 14 No. 12, 1163 (1969).

22. R. A. Graham, and G. E. Ingram, "Piezoelectric Current from X-Cut Quartz Subjected to Short-Duration Shock-Wave Loading," J. Appl. Phys. 43, 826 (1972).

23. R. G. McQueen, S. P. Marsh, and W. J. Carter, "The Determination of New Standards for Shock Wave Equation-of-State Work," in Behavior of Dense Media Under High Dynamic Pressures (Gordon and Breach, New York, 1968) p. 67.

24. R. N. Rogers, Los Alamos Scientific Laboratory, personal communication, 1967.

25. H. H. Cady, Los Alamos Scientific Laboratory, personal communication, 1970.

26. John M. Walsh, and Russell H. Christian, "Equation of State of Metals from Shock Wave Measurements," Phys. Rev. 97, 1544 (1955).

27. J. B. Ramsay, and A. Popolato, "Analysis of Shock Wave and Initiation Data for Solid Explosives," In Fourth Symposium (International) on Detonation, Office of Naval Research report ACR-126, p. 233.

28. Jack Jacobson and Wildon Fickett, "Plane Shock Initiation of Detonation: Computer Simulation of a Gas Gun Experiment," Los Alamos Scientific Laboratory report in preparation.

29. M. Cowperthwaite, "Determination of Energy Release Rate with the Hydrodynamic Properties of Detonation Waves," In 14th Symposium (International) on Combustion, (The Combustion Institute, Pittsburgh, 1973), p. 1259.

30. G. R. Fowles and R. F. Williams, "Plane Stress Wave Propagation in Solids," J. Appl. Phys. 41, 360 (1970).

31. Dennis Grady, "Experimental Analysis of Attenuating Wave Propagation," Poulter Laboratories Technical Report 002-72 (1972).

32. John G. Kirkwood, and William W. Wood, "Structure of a Steady-State Plane Detonation Wave with Finite Reaction Rate," J. Chem. Phys. 22, 1915 (1954), and William W. Wood and John G. Kirkwood, "Diameter Effect in Condensed Explosives: The Relation Between Velocity and Radius of Curvature of the Detonation Wave," J. Chem. Phys. 22, 1920 (1954).

33. Wildon Fickett, Los Alamos Scientific Laboratory, personal communication, 1965.

34. Evelyn Berlow, Robert H. Barth, and John E. Snow, The Pentaerythritols (Reinhold Publishing Corp., New York, 1958), p. 60.

35. Charles L. Mader, "Detonation Properties of Condensed Explosives Computed Using the Becker-Kistiakowsky-Wilson Equation of State," Los Alamos Scientific Laboratory report LA-2900 (1963), p. 105.

36. E. L. Lee, and H. C. Hornig, "Equation of State of Detonation Product Gases," in Twelfth Symposium (International) on Combustion (The Combustion Institute, Pittsburgh, Pennsylvania, 1969), p. 493.

37. Richard D. Dick, "Shock Wave Compression of Benzene, Carbon Disulfide, Carbon Tetrachloride, and Liquid Nitrogen," J. Chem. Phys. 52, 6021 (1970).

38. John Zinn and R. N. Rogers, "Thermal Initiation of Explosives," J. Phys. Chem. 66, 2646 (1962).

39. C. H. Johansson, and P. A. Persson, Detonics of High Explosives (Academic Press, London and New York, 1970), p. 94.

40. Charles L. Mader, "An Empirical Model of Heterogeneous Shock Initiation of the Explosive 9404," Los Alamos Scientific Laboratory report LA-4475 (October 1970).

41. Bobby G. Craig, Los Alamos Scientific Laboratory, personal communication, 1970.

42. M. Ya. Vasil'ev, D. B. Balashov, and L. N. Mokrousov, "Isothermal Compressibilities of Some Explosives at Pressures up to 22,000 kg cm^{-2}," Russian J. Phys. Chem. 11, 1159 (1960).

43. H. H. Cady, American Crystallographic Association, Tulane University, New Orleans, La., Winter Meeting, 1-5 March 1970, paper 18.

44. R. N. Rogers, and R. H. Dinegar, "Thermal Analysis of Some Crystal Habits of Pentaerythritol Tetranitrate," Thermochim. Acta 3, 367 (1972).

45. L. C. Myers, Mason and Hanger-Silas Mason Co., private communication (1972).

46. John Taylor, Los Alamos Scientific Laboratory, personal communication, 1972.

HK:331(70)